Journal of Power Sources 210 (2012) 101–109

Contents lists available at SciVerse ScienceDirect

Journal of Power Sources

journal homepage: www.elsevier.com/locate/jpowsour

Numerical study on the thermal management system of a molten sodium-sulfur battery module

June Kee Min [a], Chang-Hui Lee [b,*]

[a] Rolls-Royce University Technology Centre in Thermal Management, Pusan National University, San 30, Jangjeon-dong, Geumjeong-gu, Busan 609-735, Republic of Korea
[b] Research Institute of Industrial Science and Technology, San 32, Hyoja-dong, Pohang 790-600, Republic of Korea

ARTICLE INFO

Article history:
Received 1 February 2012
Received in revised form 9 March 2012
Accepted 12 March 2012
Available online 22 March 2012

Keywords:
Sodium-sulfur battery
Thermal management system
Numerical simulation

ABSTRACT

The operating temperature of sodium-sulfur battery cells is above 300 °C for use in molten liquid state electrodes. In order to achieve this high operating temperature condition in a battery module composed of multiple cells, a thermal management system, such as an electric heater and insulation, is essential. The efficiency of the module is directly dependent upon the temperature uniformity inside the module and the heat dissipation from the casing. In the present study, a new numerical model for the thermal analysis of a sodium-sulfur battery module is suggested. The equivalent thermal properties of the cell are evaluated by detailed thermal analysis on the cell. The heat generation of the cell is modeled considering the electrochemical reaction process and the variation of the resistance of the battery. Using these equivalent thermal models of the cell, a zero dimensional lumped thermal model for examining the effects of insulation and heater operation is developed. Finally, the three-dimensional temperature distribution inside the battery module is predicted by solving the thermal energy conservation equation numerically. The distribution of temperature and the thermal energy efficiency of the battery module for various design variables, such as cell arrangement and heater operations, are summarized.

1. Introduction

The sodium-sulfur battery is widely known for having a high energy density, high charge/discharge efficiency, and long cycle life. Since the fundamental research on this battery was carried out by Ford Motors [1] in the 1960s, the early studies on this battery were focused on exploiting these properties for application to electric vehicles in Europe and United States [2]. Subsequently, since the 1980s, the battery has also been considered a promising candidate for stationary energy storage. Indeed, great achievements have been made for this application, especially in Japan [3]. Recently, researchers in China [4] are also carrying out the study on the beta-alumina ceramic tubes.

The basic working principle of this battery is the electrochemical reaction between the molten sodium (cathode) and sulfur (anode) electrodes [5]:

$$2\mathrm{Na} + x\mathrm{S} \underset{\text{charge}}{\overset{\text{discharge}}{\rightleftarrows}} \mathrm{Na_2S_x} \quad (1)$$

To keep sodium and sulfur in the liquid state, the cell must be operated at high temperatures, that is, in the range 290–350 °C. At the higher end of this range (350 °C), the electromotive force (EMF) of the cell reaches 2.076 V for the two-phase region and declines to 1.78 V as the depth of discharge increases.

For a practical device, to achieve the necessary operation conditions, each battery "module," comprising multiple unitary cells, must be provided with a thermal management system including devices such as heaters and an insulating casing. According to Eck [6], this thermal management system should be able to heat the battery to the desired temperature and maintain an even temperature distribution under all operating conditions—that is, the maximum temperature difference should not exceed 25 and 20 °C in the horizontal and vertical directions, respectively. The required size of the battery module for current energy storage applications, however, continues to increase, making it increasingly more difficult to maintain temperature uniformity inside the module. Another important factor is the heat dissipation from the module, which is directly related to the module efficiency [7]. As a result, optimal design of the thermal management system for the battery module is essential for practical applications of this battery system.

To this end, numerical models that can predict the thermal performance of a battery module would be useful tools in the design of a thermal management system. Gu and Wang [8] summarized the general form of a thermal-electrochemical model for a battery system and applied it to a Ni-MH battery. Such models have also been widely used for fuel cell applications [9–11]. Indeed, several commercial computational fluid dynamics (CFD) software packages now include a specialized library module for fuel cell

* Corresponding author. Tel.: +82 54 279 6227; fax: +82 54 279 6459.
E-mail address: changhui.lee@rist.re.kr (C.-H. Lee).

0378-7753/$ – see front matter © 2012 Elsevier B.V. All rights reserved.
doi:10.1016/j.jpowsour.2012.03.028

Table 1
Specifications of the unitary sodium-sulfur cell.

	Specifications	Note
Capacity [Ah]	740.0	
Dimension [mm]	$D = 90.5/H = 542$	
Resistance [mΩ]	1.1	
Current [A]	(D/C) 80.6/(C) 71.4	
Operation	88–650 Ah	DoD 12–88%

thermal-electrochemical analysis [12]. For the sodium-sulfur battery, in particular, Hussein et al. [13] carried out a simulation to predict the voltage–current behavior and also included a simple model of the temperature variation of the module by considering the internal resistance variation.

Although there has been great progress in computer hardware performance, the current technology is not capable of including the detailed shape of each unitary cell and its corresponding heat transfer characteristics in the module calculation. The conventional alternative is to use the equivalent thermal properties [14]. This is a useful concept, especially for thermal analysis of large-scale geometries that include many periodic internal substructures with a complex configuration. Another important aspect of engineering design with numerical simulation is that the computational procedure proceeds in a stepwise fashion with several multi-fidelity sub-models. At the early stages of the design, the designer can narrow down the important design variables by using low-fidelity solvers that can analyze many cases in a relatively short period. As a result, the number of analyses required for the time-consuming detailed high-fidelity solver can be minimized. This multi-step and multi-fidelity approach is the key strategy for systematic engineering design.

This paper presents such a numerical prediction model for sodium-sulfur battery modules. The equivalent thermal properties for a unitary cell are evaluated by solving the steady-state heat transfer problem. Then, for the entire module, three multi-step computational models are proposed. The low-fidelity models adopt lumped capacitance assumptions, and the final high-fidelity model can predict the detailed thermal performance of the module. Thermal analysis on a typical sodium-sulfur battery module was carried out using the proposed method. The effects of the insulation wall and heater operation, module efficiency, and the temperature distribution inside the module are summarized quantitatively.

2. Development of numerical models

Fig. 1 represents the configurations of the sodium-sulfur cell and module considered in this study. Basically the model was taken from the open literature [15,16] presented by NGK Insulators. Fig. 1(a) shows the size and internal shape of the unitary cell, which contains the sodium electrode in the core, the electrolyte made of beta-alumina, and the sulfur electrode surrounding the electrolyte. It was assumed that the sodium cartridge is made of stainless steel (STS430) and the material of the cell container is aluminum (AL3003). By connecting these cells, the module, which has a capacity of 360 kW h, was modeled as shown in Fig. 1(b), which represents the in-line cell arrangement at the horizontal mid-plane of the module. The casing of the module is made of insulation material. It is assumed that the gaps between the cells are completely filled with engineering sand made of SiO_2. The detailed specifications of the cell and module used in the present analysis are summarized in Tables 1 and 2, respectively. For the information not specified in Refs. [15,16], commercially available data are assumed. For the discharge and charge period, constant current operation is assumed.

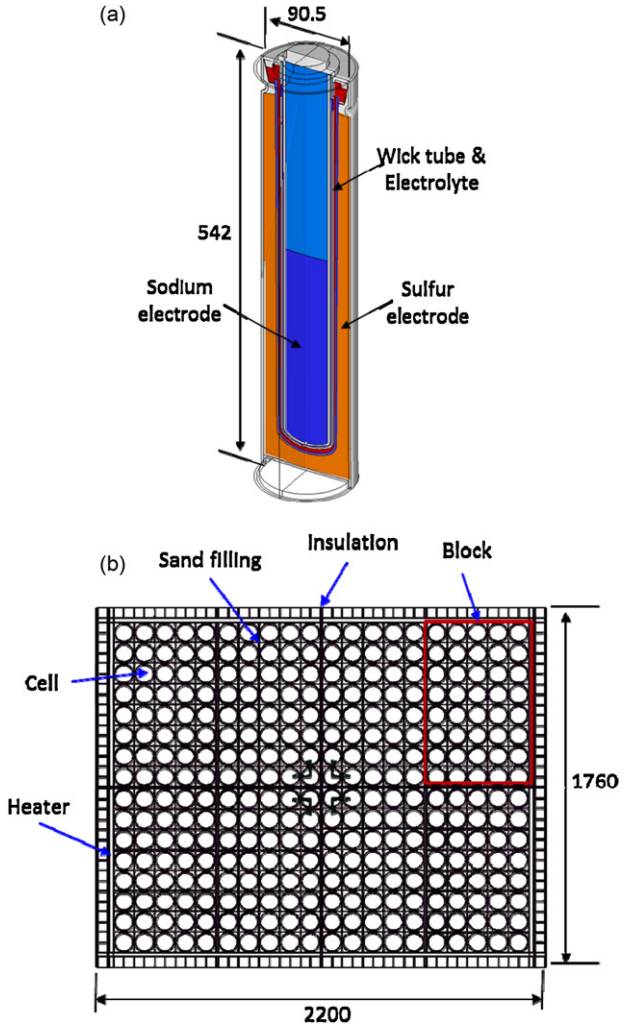

Fig. 1. Configurations of the sodium-sulfur battery cell and module considered in this study: (a) the half-cell configuration and (b) the horizontal mid-plane of the module.

As a systematic numerical approach to predicting the performance of a thermal management system, "multi-step and multi-fidelity" numerical models are proposed in this paper. There are a cell model and a module model for the thermal analysis. The module model has three steps, (i) the steady-state lumped model, (ii) the transient lumped model, and (iii) the detailed three-dimensional transient model. For the transient thermal analysis, an electrochemical model for the evaluation of cell heat generation is used.

2.1. Cell model

The purpose of the cell analysis is to evaluate the equivalent thermal properties of the unitary cell: the thermal conductivity,

Table 2
Specifications of the sodium-sulfur battery module.

	Specifications	Note
Configuration	8s × 5p × 8b = 320 cells	In-line arrangement
Dimension [mm]	2200 × 1760 × 650	
Power [kW]	50	
Capacity [kWh]	360	
Operation	7 h (D/C)–5 h (I)–8 h (C)–4 h (I) = 24 h	

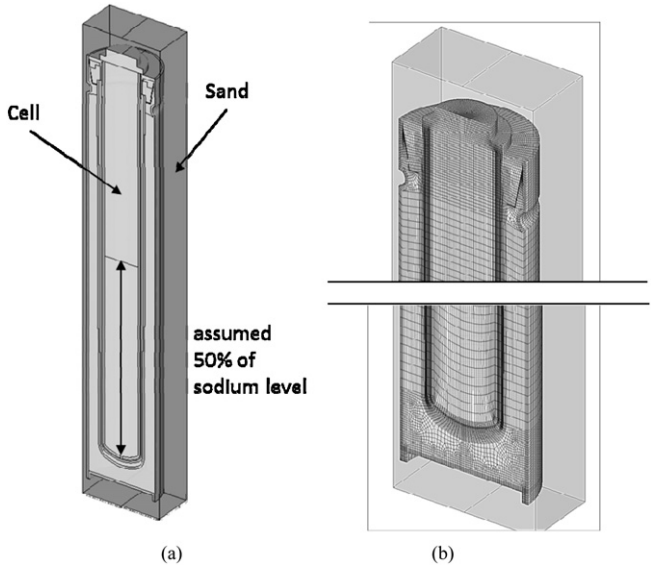

Fig. 2. Cell model for the equivalent thermal property calculation: (a) solid modeling and (b) the mesh configuration.

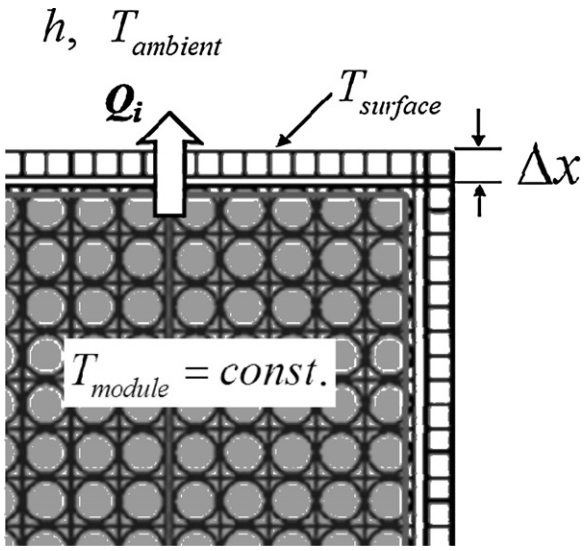

Fig. 3. Schematic of the lumped thermal model for module analysis.

specific heat, and the density. A detailed three-dimensional heat conduction analysis was adopted for this end. Fig. 2(a) and (b) shows the solid model of the cell and its corresponding mesh configuration. Using the symmetry of the geometry, only half of the cell was modeled and it was assumed that the cell was surrounded by sand. The sodium inside the core part of the cell was assumed to have a 50% level. After a detailed mesh dependency test, a total of 956 K mesh cells were generated in the computational domain. Using the commercial Computational Fluid Dynamics code ANSYS-Fluent 6.3, the following steady-state heat conduction equation was solved.

$$\frac{\partial}{\partial x_i}\left(-k\frac{\partial T}{\partial x_i}\right) = 0 \tag{2}$$

where k is the thermal conductivity of the material, T the temperature, and x_i the spatial coordinate in the i-direction. For the numerical calculation, the finite volume approach using a second-order central difference scheme was used.

As it can be seen from the cylindrical geometry of the unitary cell, the thermal conductivity of the cell should be different in the vertical and horizontal directions. In other words, the thermal conductivity should have an anisotropic or an orthotropic property. In the present calculation, it is assumed that there is an artificial temperature difference in the vertical and horizontal directions, respectively. The equivalent thermal conductivity of the computational model in the i-direction $k_{\text{model},i}$ can be evaluated using the following Fourier's law of conduction.

$$Q_i = k_{\text{model},i} A_i \frac{\Delta T_i}{\Delta x_i} \tag{3}$$

where Q_i is the heat transfer rate, A_i the cross sectional area, ΔT_i the temperature difference, and Δx_i the length of the model in the i-direction, respectively. The conductivity of the model can be expressed using the volume fraction of the cell α:

$$k_{\text{model},i} = (1-\alpha)k_{\text{sand}} + \alpha k_{\text{cell},i} \tag{4}$$

$$\alpha = \frac{Vol_{\text{cell}}}{Vol_{\text{model}}} \tag{5}$$

Here, Vol_{cell} and Vol_{model} represent the volume of the cell and the total computational domain, respectively. Using Eq. (4), the equivalent thermal conductivity of the cell can be calculated by applying the finite temperature difference in the vertical and horizontal directions as the boundary condition. At the other sides of the domain, the thermally adiabatic condition is applied. The other equivalent thermal properties, such as the density and the specific heat of the cell, can be calculated by the volume average of each part of the cell.

2.2. Steady-state lumped thermal model

The determination of insulation material and its geometric specifications such as the thickness is one of the most important steps in the design of the thermal management system for the battery module. Assuming the module temperature is constant inside the casing, as shown in Fig. 3, the heat dissipation from the module on the i-th side can be calculated by solving the following equation.

$$\begin{aligned} Q_{\text{dissipation}} &= \sum k_i A_i \frac{T_{\text{module}} - T_{\text{surface},i}}{\Delta x_i} \\ &= \sum h_i A_i (T_{\text{surface},i} - T_{\text{ambient}}) \end{aligned} \tag{6}$$

where k_i is the thermal conductivity of the insulation material, Δx_i the thickness of the insulation, h_i the convective heat transfer coefficient of i-th side of the module, respectively. A simple calculation program has been generated for this prediction. By changing the thermal conductivity of the insulation, the thickness of insulation, and the ambient cooling conditions, the total amount of heat transfer and its distribution on the surfaces of the module can be predicted.

2.3. Electrochemistry of the battery cell

For the transient thermal analysis of the module, the heat generation inside each cell should be taken into consideration. The heat generation inside the cell can be represented by following equation [17–19].

$$Q_{\text{cell}} = Q_{\text{joule}} + Q_{\text{reaction}} = I\left(\eta - T\frac{dE}{dT}\right) \tag{7}$$

where I is the current, η the polarization and (dE/dT) is the temperature dependence of the open circuit voltage. The first term of Eq. (7) represents the joule heating due to the electric resistance of the cell, and the polarization is written by

$$\eta = IR \tag{8}$$

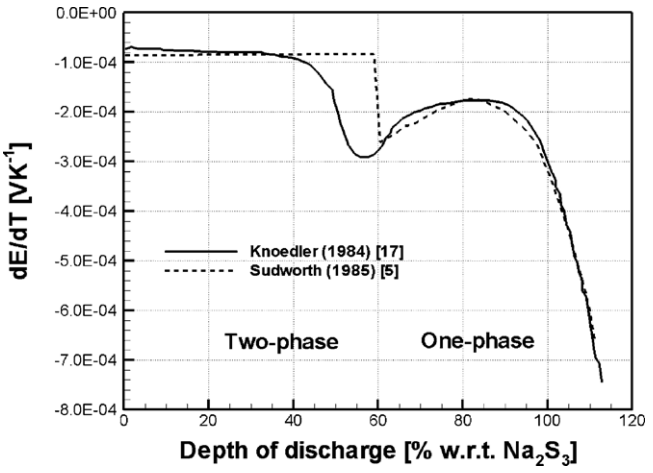

Fig. 4. Variation of the entropy term of the sodium-sulfur cell reaction.

$$Q_{joule} = I^2 R \tag{9}$$

where R is the electric resistance of the cell. During the discharge and charge process, this resistance value varies according to the depth of discharge (DoD). For large capacity battery, this is mainly caused by the variation of the reaction surface inside the cell. For poorly designed capillary wick tube inside the cell, the cell resistance increases as the area of the reaction surface on the electrolyte decreases. The resistance variation can be obtained from the unitary cell experiment measuring the voltage at a constant current using the following equation:

$$R = \frac{OCV - V}{I} \tag{10}$$

where OCV is the open circuit voltage and V is the measured voltage. In the present study, the variation of resistance, which is calculated by Eq. (10), is used in the calculation.

The second term in Eq. (7) is the heat of reaction term and $T(dE/dT)$ is called the entropy term. There have been several experimental approaches to evaluate this entropy term using adiabatic discharge/charge measurement [5,17,18]. Fig. 4 represents the typical variation of the entropy term taken from previous studies. At DoD = 60%, there is a sudden change of the pattern and this is due to the transition between the two-phase and single-phase regions. It should be noted that this sodium-sulfur reaction is exothermic for the discharge process and endothermic for the charge process, respectively. In the present calculation, the reaction model suggested by Knoedler [17] was adopted for the transient thermal analysis.

2.4. Transient lumped thermal model

It is well known that the lumped heat transfer model always gives efficient results for the thermal design [12] as shown in the steady-state lumped thermal model. By extending the concept to the transient case, the average temperature variation of the module according to the discharge and charge operation schedule can be predicted efficiently. This calculation can evaluate the module efficiency considering the heat dissipation loss as well.

Assuming a uniform temperature inside the module, the governing equation for the transient heat balance of the module can be written as

$$\begin{aligned} \rho C_p Vol \frac{dT}{dt} &= Q_{heater} + Q_{joule} + Q_{reaction} - Q_{convection} \\ &= Q_{heater} + I\left(\eta - T\frac{dE}{dT}\right) - \sum h_i A_i (T_{surface} - T_{ambient}) \end{aligned} \tag{11}$$

where ρ and C_p are the equivalent density and specific heat of the module, respectively, and Q_{heater} is the amount of heat by electric heater. To solve this zero-dimensional ordinary differential equation, a numerical code was developed using an explicit time integration scheme. The present tested battery module has 24 h operation schedule which is shown in Table 2. The average temperature of the module and its corresponding heat generation and dissipation were predicted over this period.

2.5. Three-dimensional thermal model

The final step of the calculation is the three-dimensional transient thermal model that predicts the detailed temperature distribution inside the module considering a three-dimensional geometric effect.

Assuming the gap in the module is completely filled with sand, the governing equation for the conduction analysis is written as

$$\frac{\partial}{\partial t}(\rho C_p T) = -\frac{\partial}{\partial x_i}\left(-k\frac{\partial T}{\partial x_i}\right) + q_s''' \tag{12}$$

where q_s''' is the volumetric heat source term. When there is empty space inside the module that is not filled with sand, there should be natural convection of air and the transient computation with convection becomes extremely time-consuming. In the case, however, the concept of effective thermal conductivity [20] for the convection region would be applicable to the transient conduction analysis. The same numerical scheme used for the cell model is also used in the analysis and the implicit time integration is carried out numerically. To impose the Joule heating, the cell reaction and the electric heating in the heat source term for each control volume of the generated mesh, a numerical code was developed to customize the commercial code Fluent 6.3 using the User Defined Function (UDF) capability of the program.

Fig. 5(a) shows the solid model of the current tested module. Using the symmetry of the geometry, only a quarter part of the module is modeled. Fig. 5(b) represents the corresponding mesh configuration of the quarter model, which has 1.2 M hexahedral control volume. In the model, the cells are assumed to have the equivalent thermal properties evaluated in the cell model calculation.

In all the calculations, the ambient temperature is set to $T_{ambient} = 20\,^{\circ}C$ and the convection heat transfer coefficient is $h = 5\,W\,m^{-2}\,K^{-1}$. The internal temperature of the steady-state lumped model T_{module} was assumed to have 350 °C, and the initial temperature of the transient lumped model T_{module} was set to 310 °C. Since the current thermal models consider the conduction heat transfer only, and the internal heat generation of the cell due to the electric resistance and electrochemical reaction is very slow, the time step for the present numerical integration could be relatively large compared to the heat transfer problem with convection. Szabo [21] summarized the necessary time step size for numerical stability. In the present transient calculations, a time step of $\Delta t = 5$ s was enough to satisfy the stability criterion and independency of the time step size.

3. Results and discussion

3.1. Equivalent thermal property of the cell

Fig. 6(a) and (b) shows the calculated temperature distributions inside the cell for vertical and horizontal temperature loadings, respectively. The temperature difference in each direction was set to 100 °C. Using the method described in the previous section for the cell model, the orthotropic thermal conductivity was evaluated. Fig. 7 represents the calculated thermal conductivities in

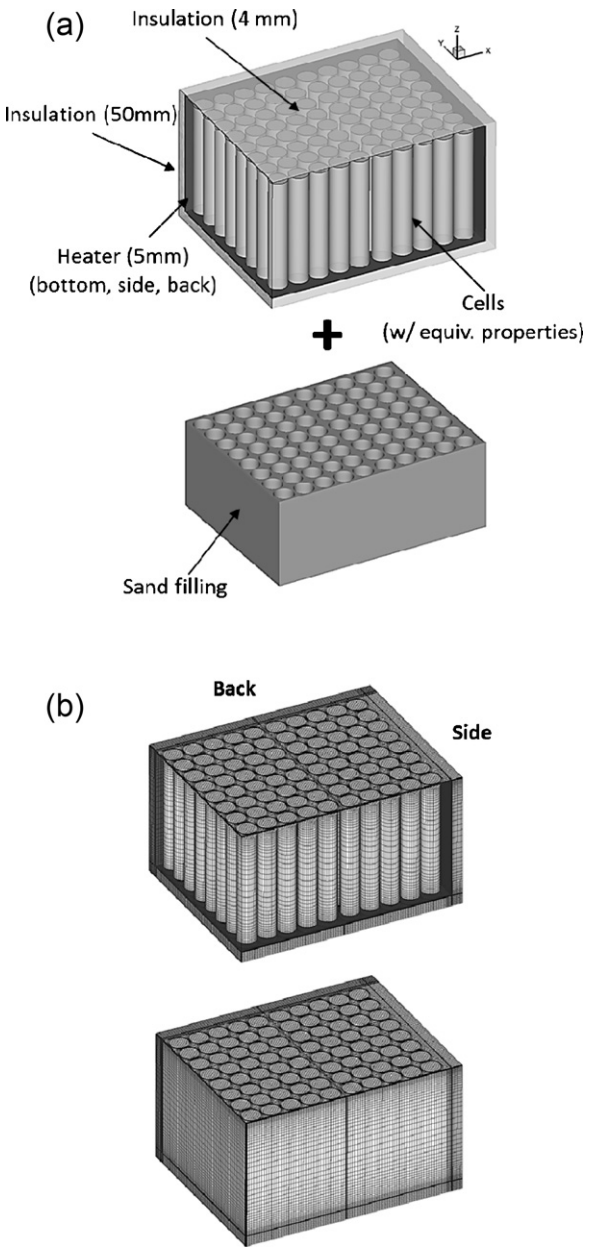

Fig. 5. Module model for the detailed 3D calculation: (a) solid modeling and (b) mesh configuration.

the vertical and horizontal directions with different casing materials. Here, the conductivity is normalized by the volume average value of the thermal conductivity of the cell. The normalized values are much smaller than unity, which represents the importance of the current cell model approach to get the direction dependent thermal conductivity. The conductivity in the vertical direction shows a larger value than that of the horizontal direction. For a stainless steel casing it is larger by 170% and for aluminum casing by 123%. This is due to the cylindrical shape of the internal structure. The shell type internal casing and electrolyte, which are aligned parallel in the vertical direction, deliver the heat along the longitudinal direction. In the horizontal direction, however, each component is separated by the others, which results in a larger thermal resistance connected in series. When the casing material is changed to aluminum, there is an increase of conductivity by 36% and 64% in the horizontal and vertical directions, respectively. The other thermal properties, such as density and specific heat, can be

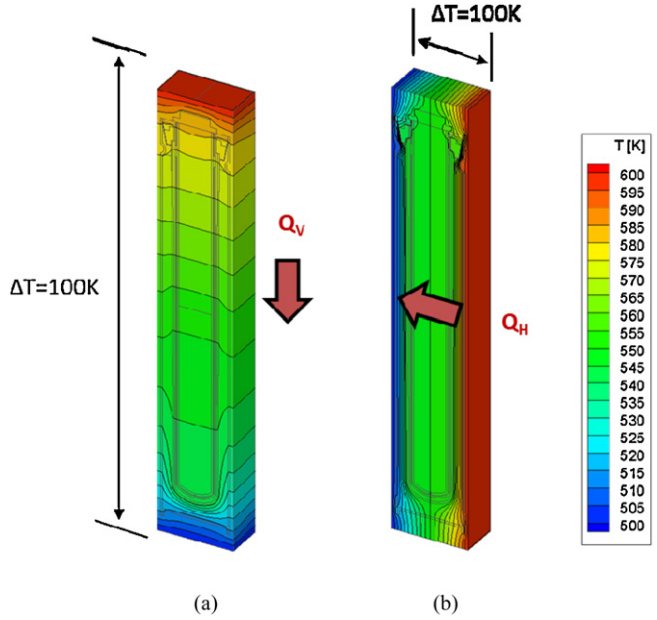

Fig. 6. Temperature distribution inside the cell under: (a) vertical temperature loading and (b) horizontal temperature loading.

calculated by taking the volume average values and using the volume fraction relation. The baseline cell model made of aluminum casing in the present study has an equivalent thermal conductivity of 5.39 W m^{-1} K^{-1} and 2.42 W m^{-1} K^{-1} in the vertical and horizontal directions, respectively. The equivalent density and the specific heat are 2247.1 kg m^{-3} and 1103.8 J kg^{-1} K^{-1}, respectively.

3.2. Heat balance and insulation

NGK insulators [15] reported that the insulation of the top face of the module should be thinner than other faces in order to reduce the temperature difference in the horizontal direction. In the current calculation using a steady-state lumped model, two different insulation thicknesses were tested: (i) 50 mm for everywhere except the top face which has 4 mm (baseline model) and (ii) 15 mm everywhere. For the insulation material, the typical thermal conductivity of vacuum insulation was used (k = 0.01 W m^{-1} K^{-1}). These two types of insulation thickness were selected based on the heat dissipation capacity described in NGK reference [15], which has the range of 2200–3200 W. In the present paper, the insulation thicknesses were selected to have the dissipation of 2700 W (the mean value) by several iterations. Table 3 indicates the distribution of heat dissipation from the module. The heat dissipation through each face is directly proportional to the thermal conductivity of

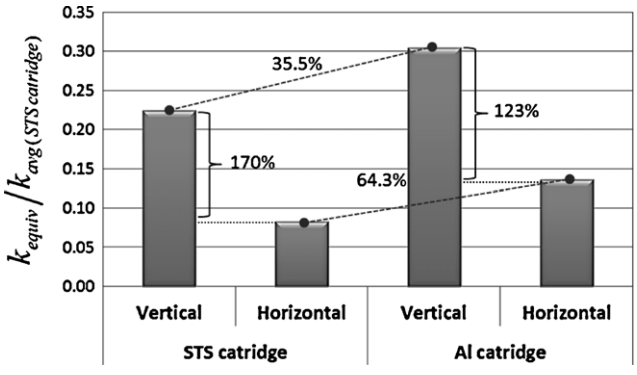

Fig. 7. Dimensionless equivalent thermal conductivity of the cell.

Table 3
Distribution of heat dissipation from the module for different insulation thicknesses [%].

Faces	Top = 4 mm Else = 50 mm	15 mm everywhere
Top	78.8	30.0
Bottom	9.1	30.0
Left	2.7	8.9
Right	2.7	8.9
Front	3.4	11.1
Back	3.4	11.1

the insulation, area of the face, and the reciprocal of insulation thickness at a given external cooling and internal temperature. As represented in the table, for a thin top wall, 78.8% of the heat is dissipated from the top surface as it was intended. If the module used uniform insulation thickness for all the face, the distribution directly follows the area ratio as is shown in the second column of the table, while the total amount of heat transfer rate of 2700 W is almost the same as that for a thin top wall. The effect of the insulation material property on the total heat dissipation was also examined. If the thermal conductivity of the insulation wall was changed to 0.023 W m^{-1} K^{-1}, the total heat dissipation became 4670 W. This prediction is helpful for designing heater capacity at the early stage of the module design.

3.3. Temperature variation and heater operation

In the transient lumped thermal model for the battery module, the ideal heater operation can be evaluated by considering the heat balance between heat generation in the cell and the dissipation from the module. Table 4 indicates this ideal minimum heater operation of the tested module. Fig. 8(a) shows the amount of heat generation and dissipation of the baseline module, and the variation of module temperature for a 24 h cycle is shown in Fig. 8(b). During the discharge period, the amount of heat generation due to the Joule heating and reaction heating inside the cells is larger than that of heat dissipation from the casing. This excessive internal heating results in an increase of module temperature and there is no need for additional heating by electric heaters. In the first idle period (Idle#1), the elevated temperature decreases by the external cooling. At the end of the first idle process, however, the average temperature of the module is still higher than the initial temperature, so the heater should be off for this period as well. In the charge process, although the endothermic reaction occurs in the cell, due to the Joule heating and higher initial temperature, the temperature does not decrease lower than the initial temperature. Finally, in the second idle period that completes the 24-h cycle, the heater operation is necessary to prevent a temperature decrease below the initial temperature. The exact capacity of the heater can be calculated using the heat balance after several iterations.

In Fig. 8(b), the circular symbol represents the experimental data from Refs. [15,16]. The time averaged difference of temperature between the calculation and measurement is 5 °C. Considering the limited information in Ref. [15], the agreement between the two is good. The detailed information, however, such as the environmental conditions of the module under operation, the location of temperature measurement sensors, the capacity of the heater and its operation schedule, and the thermal properties of the insulation wall could improve the agreement better.

Table 4 also contains the heater operation when the insulation material has larger thermal conductivity values (k = 0.023 W m^{-1} K^{-1}) and the resulting temperature variation is shown in Fig. 8(b) with the dotted line. Due to relatively poorer insulation capability, the heat dissipation becomes larger than in the case of baseline. As a result, the heater operation is necessary from the first idle period. During the charge process, it can be seen from the figure that there is a region in which the temperature drops below the initial temperature due to the endothermic reaction. After the whole cycle, however, the temperature recovers the initial level since the heater capacity was set to balance the dissipation and generation.

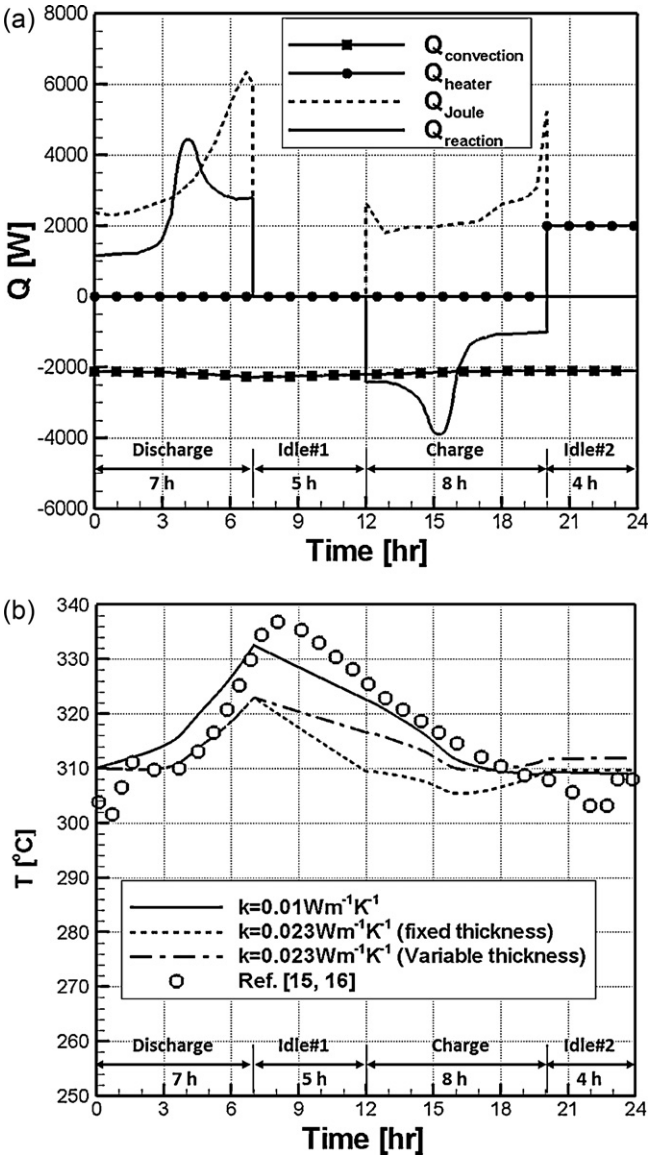

Fig. 8. Results of the transient lumped model for the baseline module (k = 0.01 W m^{-1} K^{-1}): (a) the heat generation and dissipation of the module and (b) variation of the module temperature for the 24 h cycle.

3.4. Efficiency consideration and variable insulation thickness

As summarized by Okuyama and Nomura [7], the efficiencies of the battery and the module are represented as follows:

$$\eta_1 = \frac{A}{B} \tag{13}$$

$$\eta_2 = \frac{A}{B + C} \tag{14}$$

where A is the discharge energy output, B the charge energy input, and C the heater power consumption. The efficiencies of the tested models in this study are also represented in Table 4. When the

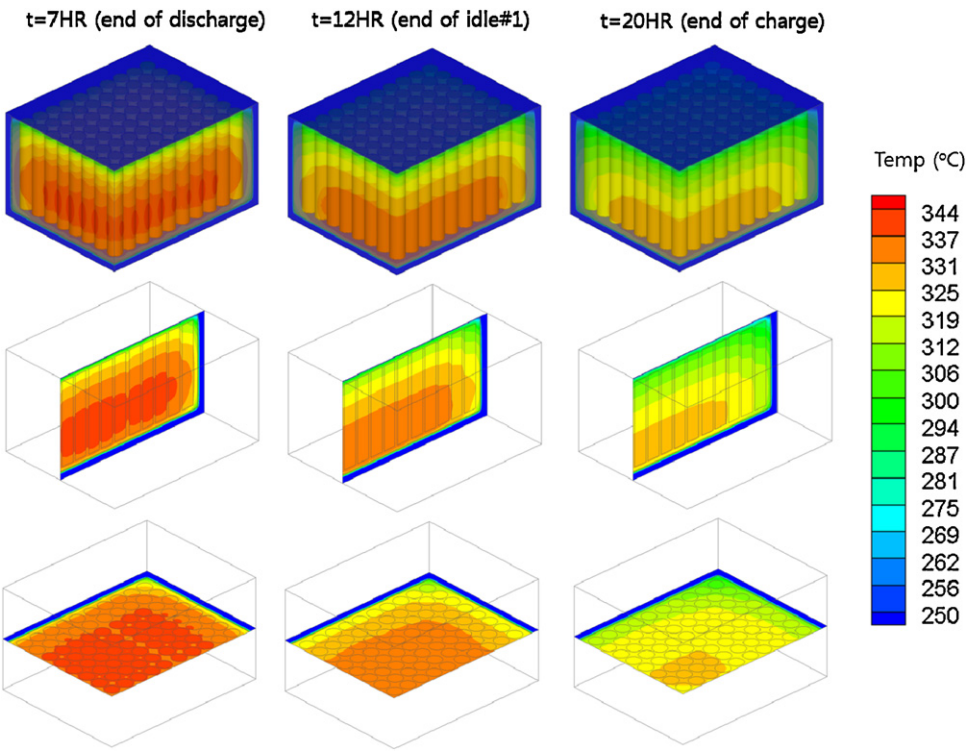

Fig. 9. Temperature distribution inside the baseline module for various times at the symmetric planes, the vertical mid-plane, and the horizontal mid-plane.

insulation has lower conductivity ($k = 0.01\ \mathrm{W\,m^{-1}\,K^{-1}}$), the module efficiency is close to the battery efficiency. With poorer insulation ($k = 0.023\ \mathrm{W\,m^{-1}\,K^{-1}}$), however, the module efficiency decreases by 9%, which was caused by the additional heater operation. It should be noted that the current module efficiency is the ideal (theoretical) efficiency since the minimum heater operation was assumed at the given condition. In real operation conditions, the module efficiency should usually be smaller than this ideal one because of the variation of external conditions. The active control of heater operation by monitoring the module temperature is essential for practical and reliable operation. Nonetheless, still the current ideal module efficiency is important for the thermal design as it represents the fundamental performance of the module system.

The concept of using variable conductance insulation for the battery module is to optimize the dissipation of heat from the casing by controlling the conductivity of the material. The necessary optimal heat dissipations from the casing for the discharge period should be larger than those for the charge and idle processes because of exothermic internal cell heat generation. According to the previous studies, the control of heat dissipation was possible by changing the pressure level inside the vacuum insulation panel [22]. The same effect is also possible by changing the thickness of the casing which has fixed thermal conductivity, as the heat transfer rate through the insulation wall is proportional to the thermal conductivity and the reciprocal of thickness. In the present study, the variable thickness model was tested, and the results are indicated in the last column of Table 4. In the calculation, the upper thickness was set to 4 mm for the discharge process and set to 50 mm for other periods, which has the same meaning as the conductivity decreased to 8% of the original value by changing the vacuum level. The result shows there is a great improvement in the module efficiency, i.e., the efficiency of 78% for fixed thickness increases to 85.8%. The corresponding temperature variation is also shown in Fig. 8(b) with a dash-dot line. It is obvious that the case of the variable insulation thickness shows the smallest temperature variation of the module.

3.5. Temperature uniformity inside the module

Fig. 9 shows the temperature distribution inside the module at the end of discharge ($t = 7$ h), the end of the first idle period ($t = 12$ h), and the end of the charge period ($t = 20$ h). The temperature becomes highest at $t = 7$ h due to the excessive internal heating, and decreases as the cycle goes since the heat dissipation by external cooling is larger than the internal heat generation for the rest of the process. The thin top wall allows the largest heat dissipation through the wall. As a result, the temperature gradient in the

Table 4
Module and ideal heater operations for different insulations.

Mode	Time [h]	Heater operation [W]		
		$k = 0.01\ \mathrm{W\,m^{-1}\,K^{-1}}$ (baseline)	$k = 0.023\ \mathrm{W\,m^{-1}\,K^{-1}}$ (fixed thickness)	$k = 0.023\ \mathrm{W\,m^{-1}\,K^{-1}}$ (variable thickness)
Discharge	7	0.0	0.0	0.0
Idle_1	5	0.0	680.0	0.0
Charge	8	0.0	3360.0	442.0
Idle_2	4	2000	3660.0	1426.0
$\eta_1 = A/B$		87.8%	87.8%	87.8%
$\eta_2 = A/(B+C)$		86.0%	78.7%	85.8%

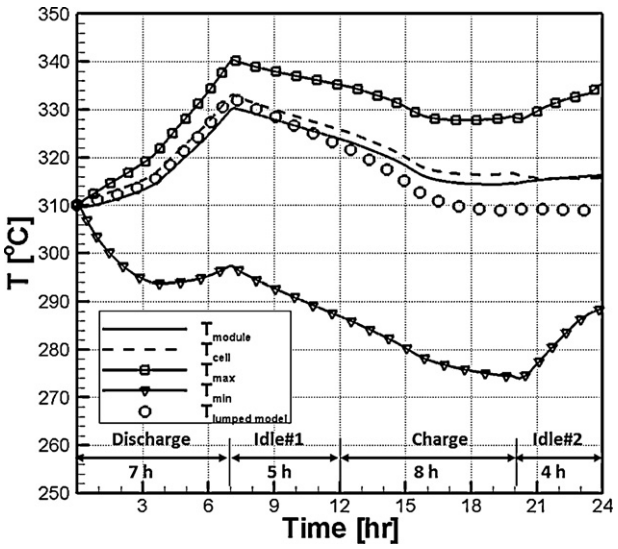

Fig. 10. Variation of the average, maximum, and minimum temperatures for a 24 h module cycle.

vertical direction is larger than that in the horizontal direction as it was intended. Since the equivalent thermal conductivity of the cell is larger in the vertical direction, generating larger dissipation in the vertical direction is a better strategy for minimizing the temperature gradient as much as possible. Due to the uneven insulation thickness, the maximum temperature occurs relatively near the bottom wall in the central core region. From the result of $t = 7$ h, it can be clearly seen that the temperature of the cell is higher than the surrounding sand region due to the internal heat generation by resistance and battery reaction. In the horizontal direction, the internal temperature decreases from the center to the side wall gradually. For the cells near the corner edge region of the module, the temperature becomes lowest, since the external cooling surface area for those cells is larger than that for other side cells. Consequently, the corner cells have the worst operating conditions, i.e., relatively lower temperature and larger temperature gradient in both directions. Since the temperature of the corner cell is largely dependent on the distance between the cell and the insulation, the gap size should be an important design variable and carefully determined.

Fig. 10 represents the variation of various representative temperatures inside the module for a 24 h cycle. The variation of the average module temperature represented by a solid line is compared with the prediction results by the transient lumped model shown by a circular symbol. The maximum difference between those two calculations was 7.5 °C and the average difference was 3.0 °C. The average cell temperature variation is close to that of the module; it is slightly higher than the module temperature for all cycle as the cell has the heat generation and heat capacity to store it. Since it was assumed that the initial temperature was uniform, the difference between the maximum and minimum temperatures becomes larger as the cycle proceeds. Even though this difference reaches 53 °C at the end of the charge process ($t = 20$ h), it should be noted that these maximum and minimum values were measured at the local extreme points inside the module. For example, the temperature difference of the cells on the horizontal mid-plane is less than 20 °C, and the vertical temperature difference on the vertical mid-plane is less than 30 °C.

In the present result for the baseline model, the heating by electric heater begins from $t = 20$ h when the charge process ends. This heating prevents the module temperature from decreasing lower than the desired level. As a result, the module and the cell temperature do not drop during the idle#2 period. The minimum temperature, however, increases rapidly since the corner cell is closely located near the heater, which represents the importance of the gap size near the side and corner region in terms of temperature stability.

Fig. 11(a) shows the temperature distribution on the horizontal mid-plane when the conductivity of the insulation wall was changed to a larger value of $k = 0.023\ \mathrm{W\,m^{-1}\,K^{-1}}$. As shown in Table 4, for this case, the heater heating should start from the charge process ($t = 12$ h) due to the large heat conduction through the casing wall. The resulting temperature distribution at $t = 20$ h is quite different from the result of $t = 12$ h. By electric heating, the temperature in the side and corner cells increases, and the variation of temperature on the horizontal mid-plane becomes smaller. In other words, the use of electric heating has a potential to improve the temperature uniformity with the penalty of module efficiency. Fig. 11(b) represents the result of temperature variation on the horizontal mid-plane of a module having a staggered arrangement of cells. When the cells are arranged in staggered way, the average gap between the cells decreases and more compact module can be constructed. The cooling rate of the module is directly dependent upon the surface-to-volume ratio. When the volume of the module for a fixed number of cell decreases, the volume ratio is proportional to the cubic power of the length scale, whereas the module surface decreases proportional to the square. Consequently, the

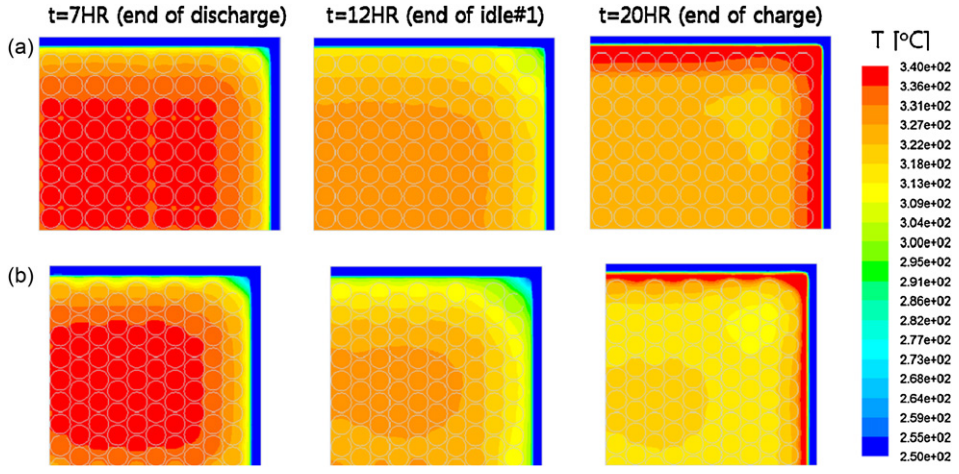

Fig. 11. Temperature distribution inside the module for different cell arrangements with an insulation of $k = 0.023\ \mathrm{W\,m^{-1}\,K^{-1}}$: (a) the in-line arrangement and (b) the staggered arrangement.

surface-to-volume ratio increases linearly to the length ratio, which means the cooling speed increases. In the present study shown in Fig. 11(b), the staggered arrangement has smaller volume by 7.9% and surface area by 6.6%. As a result, at $t = 12$ h, more cooling effect can be seen in the figure especially near the side and corner regions. In terms of temperature uniformity, the in-line arrangement has an advantage when the heater is operating, as is shown in the $t = 20$ h results. This is due to the relatively slower heat conduction speed due to larger thermal resistance and heat capacity compared to the staggered arrangement.

4. Conclusions

A fundamental analysis procedure for evaluating the thermal performance of a sodium-sulfur battery module has been developed and presented. Due to the complexity of the module, a multi-step, multi-fidelity approach is essential for the systematic design process. The proposed four-step approach is composed of (i) 3D cell analysis for evaluating the equivalent thermal properties of the cell, (ii) a steady-state lumped thermal model for estimating the heat balance and insulation thickness, (iii) a transient lumped model for determining heater operation and evaluating module efficiency, and (iv) 3D detailed analysis for predicting the temperature distribution inside the module. For the cell heat generation model, the variation of the resistance during the discharge and charge process was taken into consideration, and the electrochemical reaction term was modeled using a previous correlation for the entropy term.

Using the method suggested, the effects of various design variables were examined quantitatively. The material property of the cell and the corresponding equivalent property of the cell were evaluated for different casing materials. The orthotropic equivalent thermal conductivity of the cell shows larger conductivity in the vertical direction than in the horizontal direction. Distribution of heat dissipation on each face of the module was examined for different insulation thicknesses and materials. Module efficiency with various heater operations and insulation materials was predicted. Using the variable insulation thickness model, the improvement of module efficiency is clearly predicted. Temperature distribution inside the module for different operating conditions and cell arrangements was predicted using detailed 3D analysis. The importance of gap size at the corner and side regions and the effect of a staggered cell arrangement are found. The variation of module temperature for initial heating period to elevate the temperature from ambient to the operating temperature, and for several periods of discharge–charge cycles will be incorporated in future work.

Acknowledgements

The authors acknowledge the Research Institute of Industrial Science and Technology (RIST) for financial support. This research was also supported by the Leading Foreign Research Institute Recruitment Program through the National Research Foundation of Korea (NRF) funded by the Ministry of Education, Science and Technology (MEST) (no. K20703001798-11E0100-00310).

Appendix A. Nomenclature

A	discharge energy output, Wh
A_i	cross sectional area in the i-direction, m^2
B	charge energy input, Wh
C	heater power consumption, Wh
C_p	specific heat, $J\,kg^{-1}\,K^{-1}$
E	voltage, V
h	convective heat transfer coefficient, $W\,m^{-2}\,K^{-1}$
I	current, A
k	thermal conductivity, $W\,m^{-1}\,K^{-1}$
Na	sodium
OCV	open circuit voltage, V
q'''_s	volumetric heat source, $W\,m^{-3}$
Q_i	heat transfer rate in the i-direction, W
R	electric resistance, Ω
S	sulfur
t	time, s
T	temperature, K or °C
V	measured voltage, V
Vol	volume, m^3
x_i	spatial coordinate in the i-direction, m

Greek

α	volume fraction
Δt	time step, s
ΔT_i	temperature difference in the i-direction, K or °C
Δx_i	thickness of the model in the i-direction, m
η	polarization, V
η_1	battery efficiency
η_2	module efficiency
ρ	density, $kg\,m^{-3}$

References

[1] J.T. Kummer, N. Weber, U.S. Patent 3,413,150 (1968).
[2] Chloride Silent Power Limited, Sodium Sulfur Electric Vehicle Battery Engineering Program, DOE, report, DE-AC04-88AL54303, 1993.
[3] T. Oshima, M. Kajita, Int. J. Appl. Ceram. Technol. 1 (2004) 269–276.
[4] Z. Wen, J. Cao, Z. Gu, X. Xu, F. Zhang, Z. Lin, Solid State Ionics 179 (2008) 1697–1701.
[5] J.L. Sudworth, A.R. Tilley, The Sodium Sulfur Battery, Chapman and Hall, London, 1985.
[6] G. Eck, J. Power Sources 17 (1986) 226–227.
[7] R. Okuyama, E. Nomura, J. Power Sources 77 (1999) 164–169.
[8] W.B. Gu, C.Y. Wang, J. Electrochem. Soc. 147 (2000) 2910–2922.
[9] C.Y. Wang, W.B. Gu, J. Electrochem. Soc. 145 (1998) 3407–3417.
[10] L.-K. Chiang, H.-C. Liu, Y.-H. Shiu, C.-H. Lee, R.-Y. Lee, Renew. Energy 33 (2008) 2580–2588.
[11] H.-M. Jung, J.-Y. Koo, J. Mech. Sci. Technol. 17 (2003) 1358–1370.
[12] Fluent 6.3 User's Manual, Fluent Inc., 2006.
[13] Z.F. Hussein, L.W. Cheung, M.F.M. Siam, A.B. Ismail, Elektrika 9 (2007) 66–72.
[14] F.P. Incropera, D.P. Dewitt, T.L. Bergman, A.S. Lavine, Introduction to Heat Transfer, 5th ed., John Wiley and Sons, 2007.
[15] NGK Insulators, Development of NAS Battery Cells and Modules (in Japanese), NGK Review 60 (2005) 10–24.
[16] A. Bito, Overview of the Sodium-Sulfur (NAS) Battery for the IEEE Stationary Battery Committee Power Engineering Society General Meeting, IEEE, 2005.
[17] R. Knoedler, J. Appl. Electrochem. 14 (1984) 39–46.
[18] R. Knoedler, J. Electrochem. Soc. 131 (1984) 845–850.
[19] L. Lao, J. Newman, J. Electrochem. Soc. 144 (1997) 2697–2704.
[20] K.A. Brucker, J. Majdalani, Int. J. Heat Mass Transfer 48 (2005) 4779–4796.
[21] T. Szabo, in: S. Margenov, L.G. Vulkov, J. Waśniewski (Eds.), Lecture Notes in Computer Science 5434, Springer-Verlag, Berlin, 2009, pp. 564–571.
[22] S.D. Burch, R.C. Parish, M.A. Keyser, Thermal Management of Batteries Using a Variable-Conductance Insulation (VCI) Enclosure, NREL/TP-473-7783, National Renewable Energy Laboratory, 1995.